Pore Pressure Prediction Based on Rock Pressure Applied to Sedimentary Basins

Fernando T. B. Andrade, Lourenildo W. B. Leite, UFPA, Brazil

This paper was prepared for presentation at the 17th International Congress of the Brazilian Geophysical Society, held in Rio de Janeiro, Brazil, 8-11 November, 2021.

Abstract

This work focuses on the pressure modeling of a productive sedimentary basin. In the modeling, we calculate the vertical variation of pore, effective, and rock pressures, which serve as natural pumps for fluid accumulation, where we use post-migration surface seismic data and information as the necessary input. We compare two methods related to pore pressure calculation. In the first case, we calculate stress due to the vertical loading created by the gravitational geological overburden. In the second case, we propose a more complex method to calculate the stress distribution based on the mechanics of solids under gravity loading, using the concept of the first tensor invariant and the linear behavior of Hooke's law. We demonstrate the use of the P and S velocities and density information to calculate rock, pore, and effective pressure distributions, useful for characterizing potential zones for oil and gas accumulation. The proposed method establishes the use of the rock pressure formulation for different calculations instead of the simple overburden pressure. The combined analysis of the calculated sections serves to look for patterns and correlations, outline and characterize the target zones, and make practical geological conclusions.

Introduction

The main purpose of this work focuses on the calculation of pore pressure related to a sedimentary basin where the exploration of oil and gas is conducted. Besides, we also aim at calculating low- and high-pressure zones that serve as natural pumps for the accumulation of fluids in the subsurface. To achieve this goal, we calculate the variation of stress (and consequently pressure types) in the subsurface based on surface seismic data.

We compare two methods related to pore pressure calculation. In the first case, we calculate stress due to the vertical loading created by the gravitational geological overburden. In the second case, we propose a more complex method to calculate the stress distribution based on the mechanics of solids under gravity loading, using the concept of the first tensor invariant and the linear behavior of Hooke's law.

This work is more than a numerical experiment dedicated to pore pressure prediction, where the aim is to map pore pressure variations in the subsurface; the work is also to identify low- and high-pressure zones and correlate them to the mapped pore pressure profile. The methodology was applied to the Marmousi data, which supplies the information to construct profiles of stress prediction using V_p and V_s velocities and density ρ distributions as the necessary data as described by Sibiriakov and Sibiryakov (2015). Therefore, it is natural to classify the methodology as post-migration processing.

The methodology starts with the lithological identification to build a porosity model, followed by least-squares regression to obtain the normal compaction trend (NCT) for shales. Then, we calculate the hydrostatic pressure, the alternative overburden weight, and pore and effective pressures. The applied specific methodology results from appointed professional problems and the research literature classifies pore pressure prediction as a relevant subject in oil and gas exploration; besides, that it consists of porosity and gravity loading phenomena as described by Zhang (2013).

The used method for calculating pore pressure is based on the NCT exponential fitting as described by Athy (1930) and Zhang (2011), where is called attention to the lithologies: clay, shale, sandstone, and limestone. Several efforts are made for predicting pore pressure using porosity data. For example, Heppard et al. (1998) used an empirical porosity equation that is similar to Eaton's method using shale porosity data to predict pore pressure. We can also add the importance of the present subject to engineering aspects as given by Holbrook et al. (2005), where is described the use of petrophysical data and stress-strain relationships for pore pressure prediction in real-time drilling. Schneider et al. (2009) also describe porosity-stress relationships to predict over-pressure in claystone.

The prediction of low- and high-pressure zones and pore pressure variation in sedimentary basins for gas and oil exploration contains many theoretical aspects related to engineering, geology, and geophysics aiming to characterize potential reservoirs in the subsurface. Furthermore, the prediction and monitoring of abnormal pore pressure is a concern to avoid serious drilling incidents. The abnormally high pore pressures can cause blowouts, besides inducing geologic disasters, such as mud volcano eruptions.

Method

Solid Mechanics and Seismic Modeling

Sibiryakov et al. (2020) describe applications of the theory of solid mechanics for pressure prediction in sedimentary basins, where the purpose is to establish a mechanism for driving fluids from high- to low-pressure zones. Besides, it is necessary to analyze the participation of the so-called "effective pressure" in this fluid mechanism.

The hydrostatic pressure, P_h, is controlled by the fluid column ($h = z - z_0$) from the surface z_0 to the depth of interest z, the fluid density ρ_f, and the gravity acceleration g, expressed by the overload formula given by:

$$P_h(z) = g \int_{z_0}^{z} \rho_f(z)\, dz \;\approx\; \rho_f g h. \tag{1}$$

The overburden weight plays a role in the calculation of the normal stress, $P_z = \sigma_{zz}$ (vertical), and it is defined by the total weight of the rock formation and fluids down to the reference point, calculated by the integration of the density function to the depth z, i. e.,

$$P_z(z) = g\,\rho_{\mathsf{w}}\,h_{\mathsf{w}} + g \int_{z_{\mathsf{w}}}^{z} \rho_{\mathsf{b}}(z) dz, \tag{2}$$

where we included a liquid layer with water density ρ_{w}, height of water column h_{w}, seabed depth z_{w}, and depth of interest z.

The formation rock bulk density function, $\rho_{\mathsf{b}}(z)$, is considered to vary only with depth and given by:

$$\rho_{\mathsf{b}}(z) = [\,1 - \phi(z)\,]\,\rho_m(z) + \phi(z)\rho_f(z), \tag{3}$$

where ϕ is the porosity of the rock, ρ_m is the matrix (or mineral) density and ρ_f is fluid (water, oil, or gas) density. The bulk density can also be obtained from the density log, but these measures are not always available; therefore, we can make use of empirical prediction models.

Some authors use, and we adopt here the term *rock pressure*, P_r, defined as a simple average of the first stress tensor invariant (3D case), as given by the scalar:

$$P_r = \frac{1}{3}(\sigma_{xx} + \sigma_{yy} + \sigma_{zz}). \tag{4}$$

For the 3D geological medium case of a flat-stratified earth model, the stress is non-hydrostatic. We denominate the relevant vertical normal component stress as $\sigma_{zz} = P_z$ and a useful symmetry condition adopted is $\sigma_{xx} = \sigma_{yy}$.

Hooke's law relates linearly stress to strain. The isotropic case is given by (Fung, 1965):

$$\sigma_{ij} = \lambda\,\theta\,\delta_{ij} + 2\mu\,\varepsilon_{ij}, \tag{5}$$

where μ and λ are the Lame's elastic parameters, θ is the cubic dilation, δ_{ij} is the Kronecker delta, and ε_{ij} is the deformation tensor. Using Hooke's law (5) and the lateral symmetry $\sigma_{xx} = \sigma_{yy}$, we can show that the horizontal normal stress components are given by:

$$\sigma_{xx} = \sigma_{yy} = (1 - 2\gamma^2)\,P_z = P_x, \tag{6}$$

where the velocity ratio $\gamma = V_s/V_p$. Thus, the formula (4), for the 3D case, can be rewritten slightly different as

$$P_{rv} = \left(1 - \frac{4}{3}\gamma^2\right) P_z, \tag{7}$$

where the seismic information enters through the γ ratio. A relevant observation is related to the limitations of the models, where the layers are supposed to be horizontal or with a very smooth dip.

Effective and Pore Pressures

The effective pressure, P_{eff}, is the net pressure that acts on the solid rock matrix (skeleton) formed by the grains. According to Terzaghi (1943)'s principle, P_{eff} is defined as the difference between a general scalar overburden pressure, P_{sca} ("sca" from scalar), and the pore pressure P_p, namely,

$$P_{\mathsf{eff}} = P_{\mathsf{sca}} - P_p. \tag{8}$$

Our proposed alternative is to modify the formula (8) and use the rock pressure P_{rv}, that we can rewrite them in the form: $P_{\mathsf{eff}} = P_{rv} - P_p$.

The effective pressure is related to the part of the stress tensor which produces measurable effects such as compaction of sedimentary rocks, or an increase of shearing resistance. Thus, we can argue that P_{eff} can be considered as a driving fluid mechanism.

While compaction occurs, the sediments are buried at bigger depths, and the increase of overburden load results in a lower porosity, a lower permeability, and fluid ejection. If the sedimentation rate is higher than the fluid ejection rate from the pores, the fluids in the pores become overpressured. This compaction disequilibrium generates abnormally high pore pressure zones, with higher porosity than the normally compacted formations, as illustrates in Figure 1.

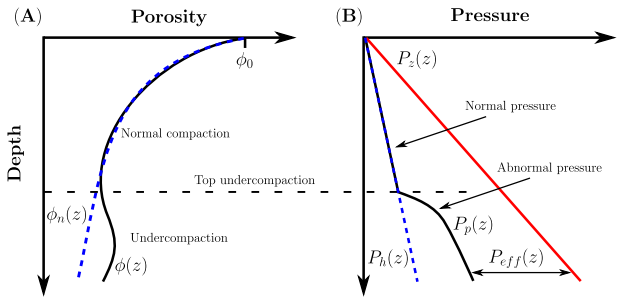

Figure 1: (A) A schematic representation of a porosity profile in a sedimentary basin. The blue dotted curve represents the normal compaction trend (NCT), $\phi_n(z)$, in a formation. The compaction disequilibrium, caused by undercompaction (black curve), generates an abnormal pore pressure profile, $P_p(z)$, as displayed in (B), which corresponds to overpressure. The details are redrawn from Zhang (2013).

Estimation of Porosity from Density

In the present case, we are interested in estimating porosity from the density profile since it is a more direct measurement. Therefore, isolating the porosity in the equation (3), we obtain the expression:

$$\phi(z) = \frac{\rho_m(z) - \rho_b(z)}{\rho_m(z) - \rho_f(z)}. \tag{9}$$

The porosity estimate from equation (9) depends on the knowledge of the fluid density in the formations, ρ_f, and the density of the matrix (or main mineral), ρ_m, for a given rock type.

NCT and Pore Pressure from Porosity and Loading

To predict abnormal pore pressure generated by the compaction disequilibrium model, we need to obtain the porosity under normal compaction conditions. Athy (1930) proposed an exponential relation for the decrease of porosity with depth under normal pressure conditions:

$$\phi_n(z) = \phi_0\, e^{-cz}, \tag{10}$$

where ϕ_n is the porosity in normal compacted formation, ϕ_0 is the porosity at the mudline (seafloor), c is the compaction factor, and z is the true vertical depth below the sedimentary depositional mudline. The law expressed by (10) is widely applied for shales because their normal porosity profiles generally show a concave downward curvature, as shown in Figure 1.

There are several methods for pore pressure prediction from formation porosity, and here we followed the method proposed by Zhang (2011), given by the optional expressions:

$$P_p^{(z)}(z) = P_z(z) - [P_z(z) - P_h(z)]\,\frac{\ln\phi_0 - \ln\phi(z)}{cz}, \tag{11}$$

$$P_p^{(rv)}(z) = P_{rv}(z) - [P_{rv}(z) - P_h(z)]\,\frac{\ln\phi_0 - \ln\phi(z)}{cz}, \tag{12}$$

where $P_p^{(rv)}$ and $P_p^{(z)}$ are the pore pressure models, P_z is the vertical overburden pressure, P_{rv} is our present proposed overburden pressure model, P_h is the hydrostatic pressure, ϕ_0 is the initial porosity (at seabed level), ϕ is the porosity at the depth of interest z and c is the compaction factor.

The main point in the interpretation for the models (11) and (12) is that the calculated pore pressure $P_p(z)$ has porosity as depth-dependent. If the porosity $\phi(z)$ (at a target depth z) is greater than the normal porosity ϕ_n for the same depth, this zone corresponds to an over-pressure; otherwise, to an under-pressure. From the concept of effective pressure, in this work, we compare the models (11) and (12) calculated with $P_{\text{sca}} = P_{rv}$ and with $P_{\text{sca}} = P_z$ and present as results.

Flowchart for Pressure Distribution Calculation

The following flowchart and block diagram of Figure 2 describes the main steps for the modelings of pore and effective pressures applied to the Marmousi2 seismic data, and it represents a summary of the methodology.

Results

Geological and Seismic Information

The model used in this work is an upgrade of the original Marmousi model, now called *Marmousi2*, as described in detail by Martin et al. (2006). The lithological composition of this model is predominantly of shale units, with occasional sand layers. The Marmousi model has a series of hydrocarbons reservoirs contained in its structural model, displayed in Figure 3. The reservoirs are distributed within a complex fault zone at varying depths, also in the layers with simple structural settings and more structurally complex locations, as folds.

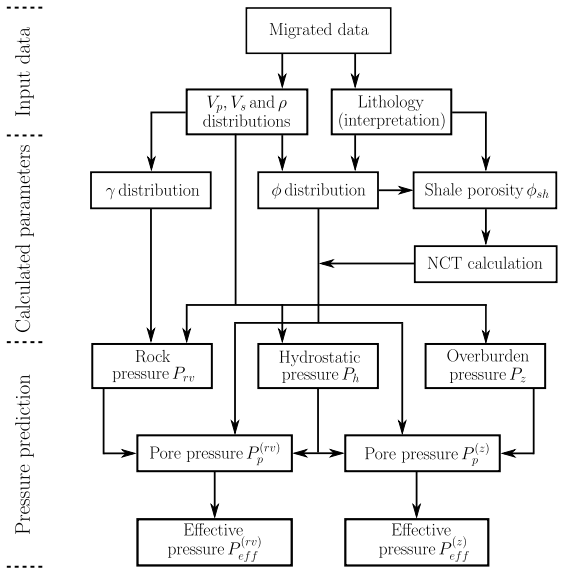

Figure 2: Block diagram showing the main steps of the pore pressure prediction and the relationships between the input data, calculated parameters, and pressure sections.

The available data has seismic velocities (V_P and V_S) and density (ρ) distributions, necessary starting information for stress distribution calculation. The density distribution used to calculate hydrostatic (P_h) and overburden (P_z) pressure is displayed in Figure 4. Furthermore, another relevant information is the ratio distribution $\gamma = V_s/V_p$, shown in Figure 5, which participates in the modeling and represents the contribution of the seismic information for the prediction of low- and high-pressure zones and pore pressure.

In the absence of borehole data, we adopted the strategy to create a model with the lithological distinction between the main lithologies as described by Martin et al. (2006) and depicted in Figure 3, giving a constant value for each type of lithology, as described in the caption of Figure 6.

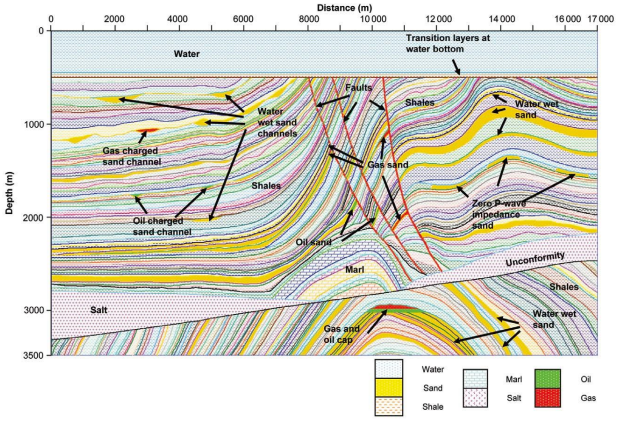

Figure 3: Structural elements, formations, and lithologies of Marmousi2 according to Martin et al. (2006).

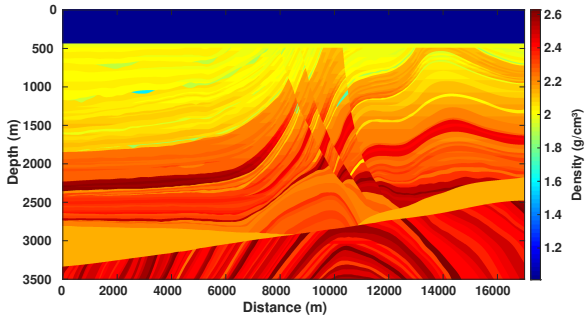

Figure 4: Density distribution $\rho(x,z)$.

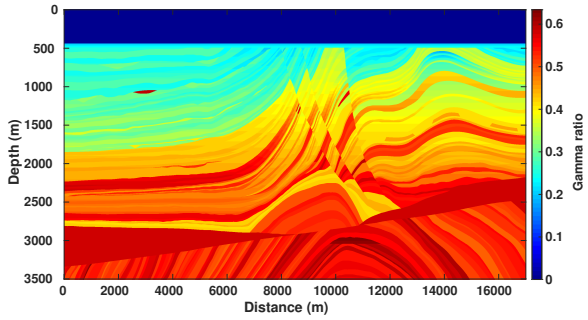

Figure 5: Gamma distribution $\gamma(x,z)$.

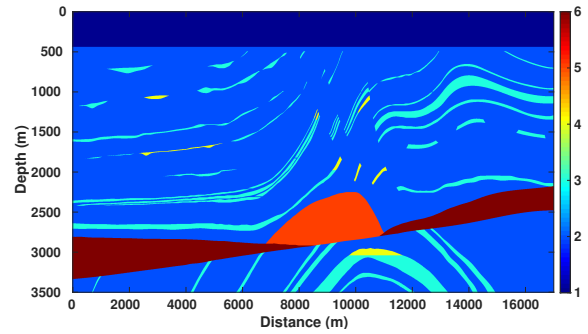

Figure 6: A lithological separation where each integer in the legend corresponds to a rock type in the following order: 1, water (dark blue); 2, shale (blue); 3, sandstone (light blue); 4, sandstone with hydrocarbons (yellow); 5, limestone (orange); 6, salt (red wine color).

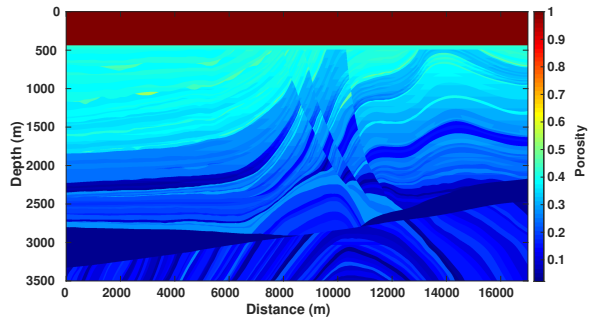

Figure 7: Section of porosity distribution $\phi(x,z)$ calculated using equation (9).

The porosity distribution was calculated from formula (9) and the model with the lithological separation, applying the matrix density values for each type of lithology.

Overburden Pressure Sections

Figure 8 shows the variation of pressure $P_z(x,z)$ according to formula (2). This map shows some details, as can be seen in the central region, where the complex fault zone is located.

On the other hand, Figure 9 represents a partial conclusion of this work, where shows the rock pressure distribution $P_{rv}(x,z)$ according to our formula (7). We notice a very different outline concerning the previous described pressure section 8.

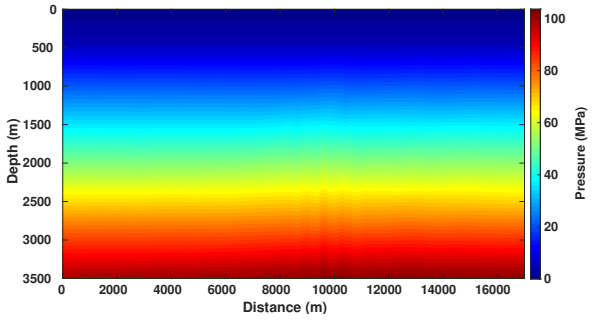

Figure 8: Section of overburden pressure $P_z(x,z)$ according to formula (2). The map is characterized by its smoothness, with some very slight variations.

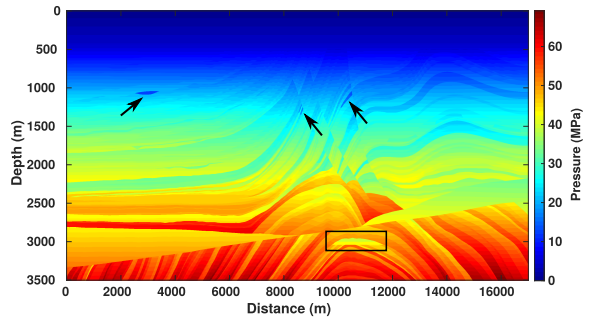

Figure 9: Section of rock pressure distribution $P_{rv}(x,z)$ according to formula (7), where we can trace the characteristics of the original geological section. The rectangle indicates the main reservoir of the basin, and the arrows indicate other smaller reservoirs. These regions correspond to low-pressure zones.

Porosity Profiles and NCT Estimation

The next step was to select some ordered porosity profiles for specific analysis and taken from the calculated model displayed in Figure 7, and shown in Figure 10. These profiles are positioned starting at 10500 m from the left border of the model, and they cross two reservoirs in different depths (1000 m and 3000 m depth).

Figure 11 shows details of the selected profiles across the main reservoir, where the porosity was calculated using formula (9). The green line represents the fit in the least-

squares sense between Athy (1930)'s exponential model and the red dots (shale formations). The obtained values for the model were $\phi_0 = 0.43367$ (fixed porosity for the mudline), and c (compaction factor) is variable (example, $c = 0.0006773$ m^{-1} for one line).

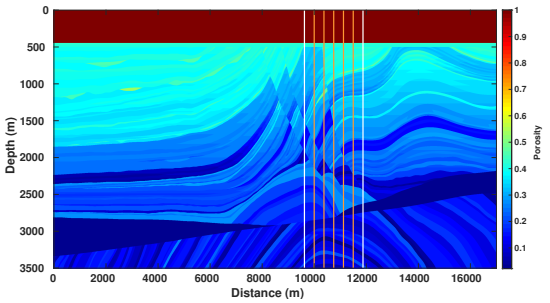

Figure 10: The selected profiles (vertical lines) over the porosity distribution displayed in Figure 7. The profiles serve for further analysis of the anticline region that includes the main reservoir (see Figure 11). The orange lines are placed over the reservoir and the white lines outside and near the reservoir.

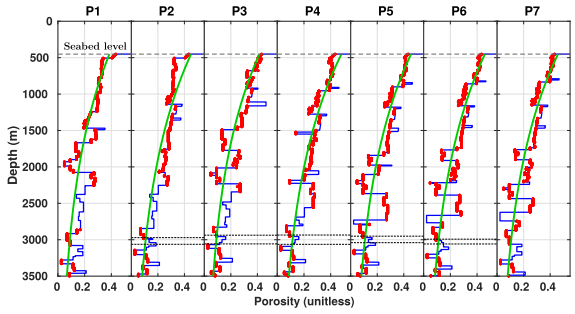

Figure 11: The porosity profiles across the main reservoir as shown in Figure 10. Blue line: complete profiles of porosity. Red dots: presence of shale formations over the blue lines. Green line: NCT for the porosity profile of the shale formations. Dashed lines: delimits in profiles P2 to P6 the reservoir zone in the anticline structure.

Pore Pressure Prediction Sections and Profiles

Figures 12 and 13 represent the sections of pore pressure calculated, respectively, by formulas (11) and (12) where we can see the good coherence between them. Also, that Figure 13 displays better the details relative to the target reservoirs, that we consider an improvement and a partial conclusion of this work.

Figures 14 and 15 represent sections of effective pressure calculated by the formula (8) with its variants (11) and (12), respectively. As in the previous case of Figures 12 and 13, Figure 15 reveals better details concerning the target reservoirs and a better color gradient for the figure. Besides, Figure 15 represents a partial conclusion in this work by highlighting better the reservoirs.

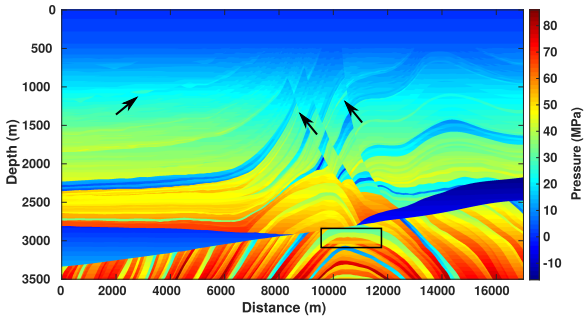

Figure 12: Section of pore pressure $P_p^{(z)}(x,z)$ based on equation (11).

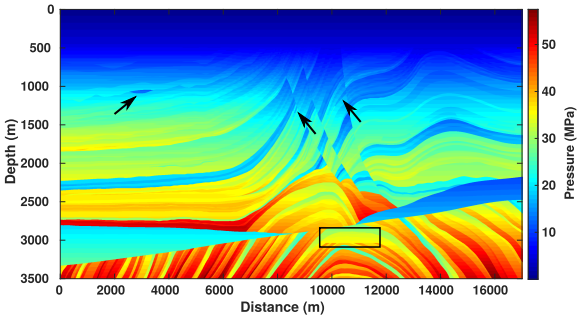

Figure 13: Section of pore pressure $P_p^{(rv)}(x,z)$ based on equation (12).

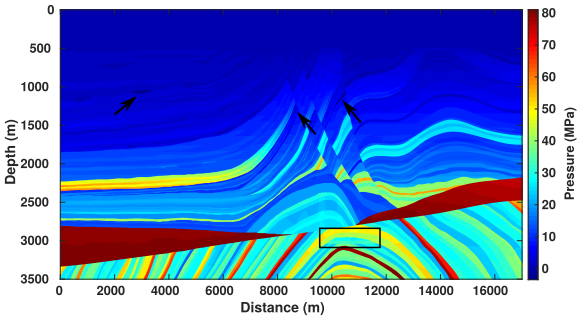

Figure 14: Section of effective pressure $P_{\text{eff}}^{(z)}(x,z)$ based on equation (8).

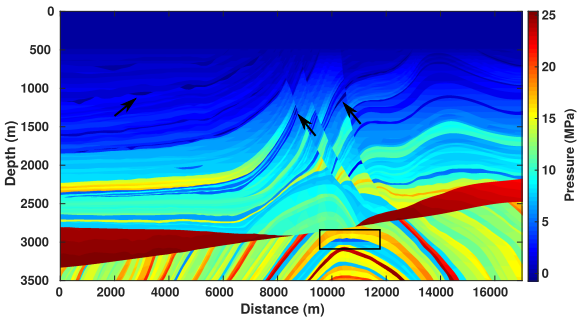

Figure 15: Section of effective pressure $P_{\text{eff}}^{(rv)}(x,z)$ based on equation (8).

For the set of profiles in Figure 16, the pore pressure varies around the reference bounds [hydrostatic (blue) and

vertical overburden (red) linear pressures]. Also, for the target reservoir located at 3000 meters depth, the pore pressure is more indicative.

For the set of profiles in Figure 17, the pore pressure varies around the reference bounds [hydrostatic linear (blue) and rock variable (red) pressures], following the tendencies of the rock pressure. Also, for the target reservoir located at 3000 meters depth, the combination of the rock pressure with the pore pressure is more indicative for the target.

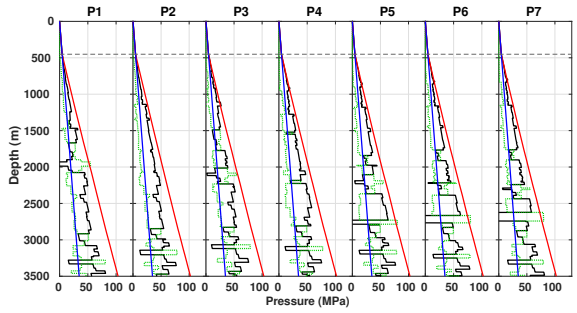

Figure 16: Pressure profiles for Figure 10. Blue: hydrostatic linear $P_h(z)$. Red: overburden linear $P_z(z)$. Black: pore variable $P_p^{(z)}(z)$. Green: effective variable $P_{\text{eff}}^{(z)}(z)$.

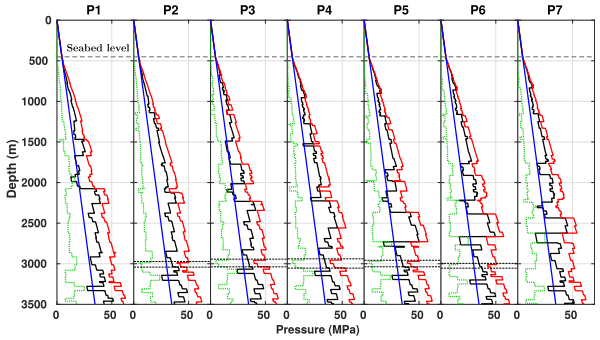

Figure 17: Pressure profiles for Figure 10. Blue: hydrostatic linear $P_h(z)$. Red: overburden non-linear $P_{rv}(z)$. Black: pore variable $P_p^{(rv)}(z)$. Green: effective variable $P_{\text{eff}}^{(rv)}(z)$. The dashed lines in profiles P2 to P6 indicates the reservoir zone contained in the anticline structure.

Conclusions

The proposed method establishes the use of the rock pressure $P_{rv}(z)$ in the models for different pressure calculations, instead of the simple overburden pressure $P_z(z)$. We demonstrated the possibility to use this method to calculate rock, pore, and effective pressure distributions, useful for characterizing potential zones for oil and gas accumulation.

The method requires the calculation of the NCT for the prediction of pore pressure. Therefore, it is necessary to know the porosity distribution values and the lithological description of the basin to identify and adjust the NCT for the same type of rock. Namely, an ill-fit curve can create false over-pressure or under-pressure zones.

It is relevant to consider a combined analysis of different pressure models to look for patterns and correlations, to outline and characterize the target zones, and to make conclusions. Therefore, we should consider the driving rock pressure, pore pressure, and effective pressure to understand the fluid percolation mechanism between low- and high-pressure zones in the basin together with the fundamentals of petroleum geology.

Acknowledgements

The authors would like to thank the Brazilian institution UFPA (*Universidade Federal do Pará*), the project National Institute of Science and Technology (INCT-GP, MCT/CNPq/FINEP), and PETROBRAS/CENPES for the research support (GEOMEC project) aiming at oil and gas exploration.

References

Athy, L. 1930. Density, porosity and compaction of sedimentary rocks. *Bulletin of the American Association of Petroleum Geologists (AAPG Bulletin)*, 14, 1-24.

Fung, Y.C. 1965. *Foundations of Solid Mechanics*, London, England: Prentice-Hall, Inc.

Heppard, P.; Cander, H.; Eggertson, E. 1998. Abnormal pressure and the occurrence of hydrocarbons in offshore eastern trinidad, west indies. *Abnormal Pressures in Hydrocarbon Environments: AAPG Memoir*, 45, 215-246.

Holbrook, P.; Maggiori, D.; Hensley, R. 2005. Real-time pore pressure and fracture gradient evaluation in all sedimentary lithologies. *Society of Petroleum Engineers*, 10, 215-222.

Martin, G.S.; Wiley, R.; Marfurt, K.J. 2006. Marmousi2: An elastic upgrade for marmousi. *The Leading Edge*, 25, 113-224.

Schneider, J.; Flemings, P.B.; Dugan, B.; Long, H.; Germaine, J.T. 2009. Overpressure and consolidation near the seafloor of brazos-trinity basin iv, northwest deepwater gulf of Mexico. *Journal of Geophysical Research*, v. 114.

Sibiriakov, E.B. and Sibiryakov, B.P. 2015. Local pressure lows as possible sinks of fluids in geologic structures. *Russian Geology and Geophysics*, 56, 1091-1095.

Sibiryakov, B.P.; Sibiriakov, E.B.; Leite, L.W.B. 2020. *Dynamics of underground rocks containing fluids. Application to exploration geophysics with emphasis on oil and gas*. Belém, Pará, Brazil: UFPA, IG, Geosciences Library, 360 p.

Terzaghi, K. 1943. *Theoretical soil mechanics*. New York: John Wiley and Sons, Inc., 510 p.

Zhang, J. 2011. Pore pressure prediction from well logs: methods, modifications, and new aproaches. *Earth Science Reviews*, 108, 50-6.

Zhang J. 2013. Effective stress, porosity, velocity and abnormal pore pressure prediction accounting for compaction disequilibrium and unloading. *Marine and Petroleum Geology*, 45, 2-11.